Available online at www.sciencedirect.com
ScienceDirect
Journal of Catalysis 249 (2007) 269–277
JOURNAL OF CATALYSIS
www.elsevier.com/locate/jcat

Structural properties of flame-made Rh/Al_2O_3 and catalytic behavior in chemoselective hydrogenation

Niels van Vegten, Davide Ferri, Marek Maciejewski, Frank Krumeich, Alfons Baiker *

Institute for Chemical and Bioengineering, Department of Chemistry and Applied Biosciences, ETH Zurich, Hönggerberg, HCI, CH-8093 Zurich, Switzerland

Received 8 March 2007; revised 25 April 2007; accepted 26 April 2007

Available online 14 June 2007

Abstract

Rhodium/alumina catalysts with Rh loadings of 0.5–5 wt% were prepared by flame spray pyrolysis, and their structural and catalytic properties were compared with that of commercial 5 wt% Rh/Al_2O_3 reference catalysts. The structure of the materials was investigated using STEM, XRD, H_2 chemisorption, TPR, and CO adsorption combined with DRIFT spectroscopy. The as-synthesized flame-made material was composed of well-dispersed oxidized 1–2 nm rhodium particles deposited on virtually nonporous agglomerated 10–20 nm alumina particles. The oxidic rhodium phase in this material showed considerably higher resistance against reduction compared with the reference catalysts up to 600 °C. On reduction, metallic rhodium and cationic Rh species were uncovered by DRIFTS. The flame-made catalysts showed an increase in the fraction of cationic species with increasing reduction temperature, whereas similar behavior was not observed with the commercial reference catalysts. The high stability of the oxidic Rh species against reduction seems to be an intrinsic structural property of the flame-made Rh/Al_2O_3 and is indicative of a strong interaction between the rhodium and alumina constituents. Although metallic Rh was a prerequisite for activity in the chemoselective and enantioselective hydrogenation of 3,5-di-(trifluoromethyl)-acetophenone, the presence of cationic Rh species seemed to positively affect catalytic performance, as shown by the superior catalytic behavior of the flame-made material compared with the commercial reference catalysts.

Keywords: Rh/Al_2O_3; Flame spray pyrolysis; Cationic Rh species; Chemoselective hydrogenation; Enantioselective hydrogenation; 3,5-Di-(trifluoromethyl)-acetophenone; CO adsorption; DRIFTS

1. Introduction

For decades, flame aerosol processes have been applied in industry for the synthesis of ceramics and such commodities as silica, carbon black, and titania [1]. More recently, these processes have gained considerable interest as elegant and relatively simple preparation methods for solid catalysts [2,3]. Gas-phase synthesis methods are intrinsically continuous, allowing easy scale-up with constant product quality. In particular, flame spray pyrolysis (FSP) [4] has emerged as an attractive synthesis method for supported noble metals [5–8], mixed metal oxides [9–12], and alloys [13,14]. The advantage of FSP over other vapor-phase synthesis methods lies in its use of non-volatile precursors, thus enhancing the scope of materials and increasing the flexibility during synthesis. Moreover, materials prepared by FSP often have been reported to have high surface area and thermal stability [6,11,15,16], both of which are desirable properties for the design of heterogeneous catalysts. Flame-made alumina-supported palladium [6] and platinum [8] have been tested in structure-sensitive reactions like liquid-phase enantioselective hydrogenation. Under optimized conditions and after reduction at high temperature (400–600 °C), improved enantioselectivity [6] and activity [8] were observed compared with commercial reference catalysts. These findings demonstrate that flame-made materials, apart from thermal stability and reducibility, can also show a different morphology and structure than traditionally prepared catalysts. This makes it interesting to explore the potential of flame-made materials in reactions in which the selectivity depends on the catalyst structure.

The synthesis of many chemicals in the fragrance, pharmaceutical, and agrochemical industries involves steps in which control of selectivity is of paramount importance. The chemos-

* Corresponding author. Fax: +41 44 632 11 63.
E-mail address: baiker@chem.ethz.ch (A. Baiker).

0021-9517/$ – see front matter
doi:10.1016/j.jcat.2007.04.021

elective hydrogenation of α,β-unsaturated aldehydes to unsaturated alcohols is an example of this, in which high selectivity toward hydrogenation of the carbonyl bond is desired [17]. Another example is the enantioselective hydrogenation of C=O and C=C bonds [18,19]. Commonly, group 10 transition metals on nonreducible supports are used for selective hydrogenation reactions, with most research to date done on Pt-based catalysts. Rhodium, although a prominent hydrogenation catalyst, is used less often for selective hydrogenations and often exhibits lower chemoselectivity compared with Pt catalysts [17]. Improved chemoselectivity can be achieved on addition of a second metal, either alloyed with Rh or present in a different form on the Rh surface.

Chirally modified heterogeneous Rh catalysts have failed to make a significant impact in enantioselective hydrogenation, because lower enantiomeric excess (*ee*) is typically obtained with Rh compared with Pt using cinchona modifiers under similar reaction conditions [20–23]. Interestingly, the reduction of Rh/Al_2O_3 at high temperature before reaction is not a prerequisite for better performance, in contrast to Pt/Al_2O_3 [20,21], representing a significant difference between Rh- and Pt-based catalysts. In the hydrogenation of aromatic ketones, Rh shows superior performance than Pt but under rather different experimental conditions [22]. In addition to commercial Rh-based catalysts, poly-vinylpyrrolidone-stabilized Rh nanoclusters were also applied in the hydrogenation of ethyl pyruvate [24]. The deposition of the nanoclusters on alumina [25] and the use of quinine or cinchonidine as stabilizing agents increased the *ee* from ca. 42% to 65% and 71%, respectively [26].

Given the surprising scarcity of data on the preparation and characterization of flame-made supported rhodium catalysts [27–29] and the scanty information available on the possible influence of the structure of rhodium on the catalytic performance in chemoselective reactions, we prepared and characterized a series of flame-derived Rh/alumina catalysts. Their catalytic potential was evaluated in the chemoselective and enantioselective hydrogenation of 3,5-di-(trifluoromethyl)-acetophenone (Scheme 1). We compared the structural and catalytic properties of the flame-derived catalysts and two commercial 5 wt% Rh/Al_2O_3 reference catalysts suitable for this type of reaction [20–22].

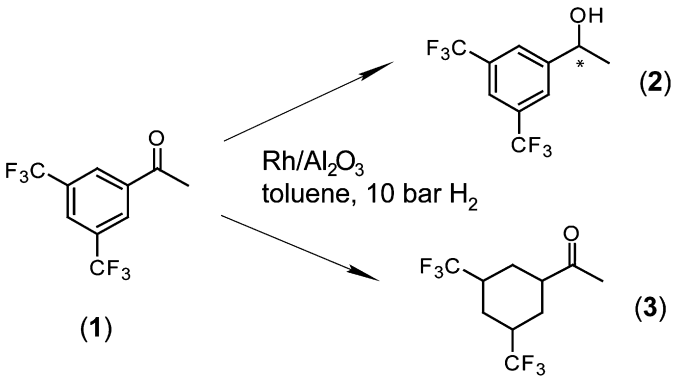

Scheme 1. Hydrogenation of (3,5)-di-(trifluoromethyl)-acetophenone (**1**) to the corresponding alcohol (**2**) and the saturated ketone (**3**) on supported Rh.

2. Experimental

2.1. Materials

Rhodium(III) acetylacetonate (97%, Acros), aluminium(III) acetylacetonate (99%, ABCR), acetic acid (analytical grade, Fluka), methanol (analytical grade, Fluka), cinchonidine (CD, 92%, Fluka), toluene (99.5%, J.T. Baker), and 3,5-di-(trifluoromethyl)-acetophenone (**1**) (98%, ABCR) were used as received. The two commercial 5 wt% Rh/Al_2O_3 catalysts used as references were Degussa G 213 RA/D (designated DG) and Engelhard 8001 Escat 34 (designated EH).

The experimental setup used for the FSP has been described in detail previously [6]. Flame-made Rh/Al_2O_3 catalysts with Rh loadings of 0.5–5 wt% were prepared by dissolving the appropriate amounts of rhodium and alumina precursor salts in a 1:1 (vol%/vol%) mixture of acetic acid and methanol. The aluminium concentration was always 0.39 M. The solution was pumped through a capillary at 5 mL/min and nebulized with 5 L_n/min O_2, and the resulting spray was ignited by a circular supporting methane/oxygen flame (1.0/0.6 L_n/min), resulting in an approximately 6-cm-long flame. Particles were collected on a cooled Whatman GF/D filter (257 mm diameter). A Busch SV 1040C vacuum pump aided in particle recovery.

2.2. Characterization

Nitrogen physisorption isotherms were measured on a Micromeritics ASAP 2010 instrument at 77 K. Samples were outgassed for 2 h under vacuum at 150 °C before measurement. Specific surface areas were determined using the BET method. Pore size distributions were calculated according to the BJH formula, using the desorption branch of the isotherm.

Hydrogen chemisorption was performed on a Micromeritics ASAP 2010C instrument. The sample was exposed to flowing hydrogen at temperatures between 100 and 580 °C for 1 h and then evacuated at the same temperature. Two chemisorption isotherms, each composed of 11 points, were then measured at 40 °C. The first isotherm corresponded to all adsorbed hydrogen. After evacuation at the same temperature for 1 h, the second isotherm was measured, corresponding to the weakly adsorbed hydrogen. From the difference between the two isotherms, the fraction of strongly adsorbed (chemisorbed) hydrogen was determined. A stoichiometric factor H/Rh of 1 [30] was assumed for calculating the dispersion of the samples reduced at 400 °C. X-ray diffractograms were recorded on a Siemens D5000 diffractometer using Cu $K\alpha_1$ ($\lambda = 1.54056$ Å) radiation in step mode between 15 and 65° 2θ with a step-size of 0.01° and 0.3 s $step^{-1}$.

For scanning transmission electron microscopy (STEM), the material was dispersed in ethanol, and some drops were deposited onto a perforated carbon foil supported on a copper grid. The investigations were performed on a Tecnai F30 microscope (FEI, Eindhoven) with a field emission cathode, operated at 300 kV. STEM images were recorded with a high-angle annular dark field (HAADF) detector, using almost exclusively

incoherently scattered electrons (Rutherford scattering) to obtain images with atomic number (Z) (cf. [31]).

Thermogravimetry (TG) combined with mass spectrometry (MS) was performed on a Netzsch STA 409 thermoanalyzer connected to a valve device, enabling pulse thermal analysis. This setup [32] allows the injection of controlled amounts (0.5–5 ml) of probe gas into a carrier gas stream flowing through the thermoanalyzer. The composition of the gas phase was monitored by a Thermostar Pfeiffer Vacuum GSD 301O1 mass spectrometer, which was connected to the thermoanalyzer by a heated (ca. 200 °C) stainless steel capillary. The pulse thermal analysis applied was based on the injection of a specific amount of gaseous reactant into the carrier gas stream and monitoring the changes in mass and gas composition resulting from the incremental extent of the reaction. Then 1-mL pulses of hydrogen were injected into the helium stream during heating at a rate of 1 K/min. After each pulse of hydrogen, leading to the partial reduction of the sample, two 1-mL pulses of oxygen were injected to fully reoxidize the sample before the next hydrogen pulse at higher temperature. Sample mass monitored online (TG curve) indicated that before the subsequent reduction process, the sample was always in the same, maximally oxidized state.

Diffuse reflectance infrared spectra were recorded during CO adsorption at room temperature with an EQUINOX 55 spectrometer (Bruker Optics) equipped with a liquid nitrogen-cooled MCT detector and an HVC-DRPZ reaction chamber (Harrick). Spectra were collected by co-adding 200 scans at a resolution of 4 cm^{-1}. Samples were diluted 1:8 with KBr and reduced in flowing 10 vol% H_2/Ar at the desired temperature for 1 h. CO adsorption was monitored over 1 h in flowing 10 vol% CO/Ar, followed by flowing Ar for ca. 30 min.

2.3. Catalytic tests

Catalytic tests were performed in a Baskerville autoclave, equipped with a 35-mm-i.d. glass sleeve and a magnetic stirrer set at 1000 rpm. The reaction mixture comprised 5 mL of toluene, 42 mg of catalyst, and 0.33 mL of substrate **1**. For the enantioselective hydrogenation, 2.0 mg of CD used as a chiral modifier was added to the previous mixture. Hydrogen pressure was controlled with a pressure controller (Büchi bpc 6002) and set at 10 bar for all experiments. Before starting the stirrer, the autoclave was flushed 10 times with hydrogen.

The catalysts were pretreated by heating ca. 120 mg of the sample to between 100 and 580 °C under flowing nitrogen for 30 min, then flowing hydrogen at the selected temperature for 1 h, and finally cooling in flowing hydrogen for 30 min. The catalysts were used within 2 h after reduction.

Conversion and enantiomeric excess (*ee*) were determined using a Thermo Finnigan Trace gas chromatograph equipped with a chiral capillary column (25 m × 0.25 mm CP-Chirasil-Dex CB, Chrompack). Selectivity to carbonyl bond hydrogenation (i.e., chemoselectivity) was calculated as $S(\%) = 100 \times \mathbf{2}/(\mathbf{2} + \mathbf{3})$. The *ee* was calculated as $ee(\%) = 100 \times (|R - S|)/(R + S)$. The selectivity to **2** was generally high, with saturated ketone as the main side product. In the absence of the chiral modifier, traces of saturated alcohol or products of hydrogenolysis were also found, and these were taken into account when calculating the selectivity.

3. Results and discussion

3.1. Structural properties

Fig. 1 shows the nitrogen adsorption–desorption isotherms of the flame-made 5 wt% Rh/Al_2O_3 (designated FM) and the corresponding commercial reference catalysts (DG and EH). The reference catalysts showed a hysteresis behavior between adsorption and desorption branches characteristic of mesoporous materials. In contrast, the adsorption–desorption isotherms of the FM sample indicate that this material does not have a well-defined mesoporous structure. The peculiar hysteresis behavior may originate from the interparticle void space between agglomerated nonporous nanoparticles. DG showed a maximum pore size distribution at ca. 11 nm, and EH exhibited a maximum pore size at ca. 5 nm. The BET surface areas of the three materials were 204 $m^2\,g^{-1}$ for FM, 117 $m^2\,g^{-1}$ for DG, and 122 $m^2\,g^{-1}$ for EH. Temperature programmed desorption (TPD) experiments performed in pure He up to 600 °C revealed removal of water and traces of CO_2, corresponding to a weight loss of 9.9% for the FM sample, compared with the reference catalysts, which showed a loss of only 4–5%.

The metal component is commonly reduced before the hydrogenation reaction [8,33]. Thus, the Rh/Al_2O_3 material prepared by FSP was characterized as prepared after reduction at 400 °C, the temperature commonly applied for hydrogen pretreatment of catalysts used in enantioselective hydrogenation [19–22].

Selected STEM images of the 5 wt% samples (before and after pretreatment at 400 °C) are shown in Fig. 2. STEM revealed no major structural changes in the materials on reduction at 400 °C. FM (Figs. 2a and 2b) showed rhodium-containing particles of 1–2 nm size deposited on agglomerated alumina particles of 10–20 nm. A few much larger rhodium particles (10–30 nm) on alumina particles of 100 nm were also dis-

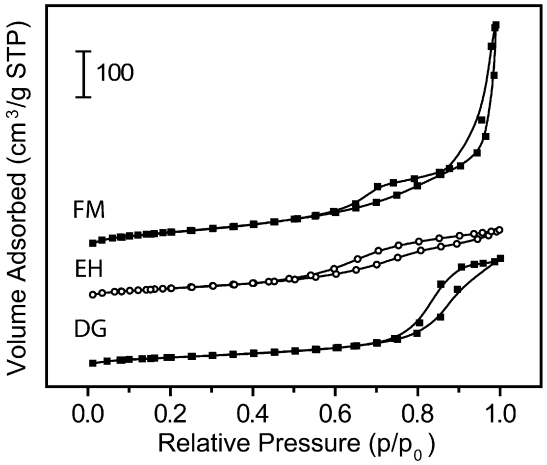

Fig. 1. Nitrogen adsorption–desorption isotherms of 5 wt% Rh/Al_2O_3 catalysts FM (▼), DG (■) and EH (○). The bar indicates an adsorbed volume of 100 cm^3/g STP.

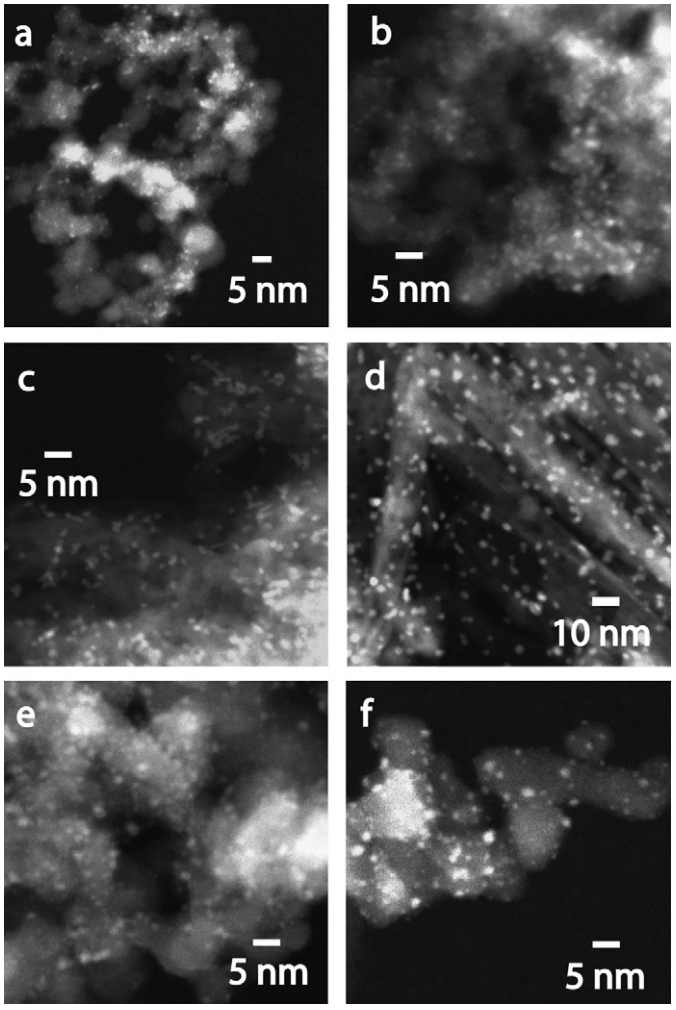

Fig. 2. Representative STEM images of the 5 wt% Rh/Al_2O_3 catalysts. Pre-treatment at 400 °C in flowing hydrogen. FM: (a) unreduced, (b) reduced; EH: (c) unreduced, (d) reduced; DG: (e) unreduced, (f) reduced.

cernible, indicating some inhomogeneity. This inhomogeneity is likely the result of the nature of the solvent mixture used during flame synthesis and can be related to the combustion enthalpy of the methanol/acetic acid mixture [15]. The as-received EH consisted mainly of well-dispersed rhodium particles (2.5–6 nm) [20], along with a considerable amount of larger particles (30–100 nm). The size distribution of the rhodium particles in DG was narrower (1–3 nm), but larger rhodium agglomerates were also found, albeit to a lesser extent than in EH.

Despite the presence of large rhodium particles in the as-received EH no rhodium-related reflections were discernible in the X-ray diffractograms (Fig. 3). This indicates that either these large particles were poorly crystalline or their amount was too low to be detected. Pretreatment in flowing H_2 at 100 °C (not shown) gave rise to a reflection at $2\theta = 41.1°$ indicative of metallic rhodium. Because at temperatures below 400 °C, no evidence of sintering was found by STEM or hydrogen chemisorption experiments (vide infra), it is unlikely that the presence of these Rh reflections resulted from sintering of rhodium particles. We attribute it instead to partial crystallization of the originally X-ray-amorphous rhodium particles. Reducing EH at temperatures above 100 °C (up to 580 °C) resulted in narrowing of the reflections with corresponding increasing intensity, indicating crystallite growth. In contrast to EH, both FM and DG showed no rhodium reflections after reduction at 400 °C, indicating that the fraction of large crystalline particles in these samples was minor compared with that in EH. Thus, we would expect only a negligible catalytic influence of sporadic large Rh agglomerates in FM, as evidenced by STEM. The diffractograms also revealed that the alumina phase present in FM and EH differed from that in DG (Fig. 3).

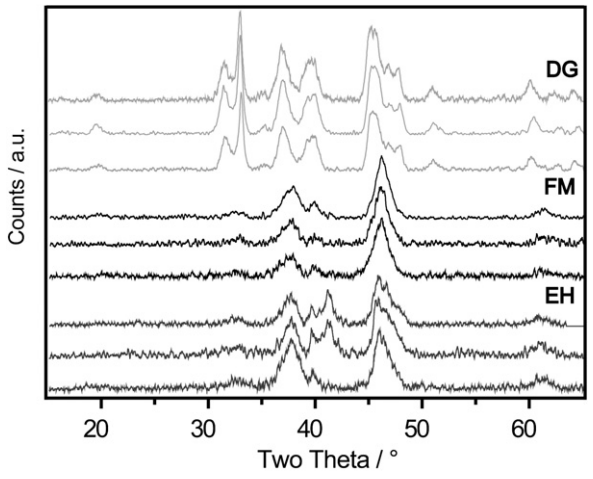

Fig. 3. X-ray diffraction patterns of DG, FM and EH as received (bottom diffractrogram), after reduction at 400 °C (middle) and after reduction at 580 °C (top diffractogram). Note that the patterns of the alumina phase in FM and EH resemble that of JCPDS 047 1308, whereas the pattern in DG are similar to that of JCPDS 011 0517.

STEM (Fig. 2) and XRD analysis (Fig. 3) indicated that FM and DG had smaller Rh particles than EH on average, and that treatment at 400 °C in flowing hydrogen did not affect this property. Because of this marked difference between the flame-made material and EH, we performed hydrogen chemisorption experiments to obtain more information on Rh particle size. In this case, the chemisorption experiments were carried out after pretreatment of the catalysts at 100–580 °C for 1 h. Fig. 4 shows that all three samples were characterized by low hydrogen uptake after pretreatment at 100 °C. After reduction at 200 °C, the uptake increased significantly for DG and EH because of the larger fraction of metallic rhodium formed at higher reduction temperatures. Further increases in the reduction temperature affected the hydrogen uptake of DG and EH only marginally. In contrast, the hydrogen uptake of FM increased up to about 400 °C, indicating the presence of more stable rhodium oxide species. At higher reduction temperatures, hydrogen uptake decreased by ca. 30%, attributed to both coalescence and sintering, which reduced the rhodium surface area. These findings are in good agreement with the reduction behavior of Rh/TiO_2 and Rh/Al_2O_3 model catalysts reported previously [34]. Surface rhodium oxide species were reduced between 100 and 150 °C. Increasing the reduction temperature up to 300 °C did not significantly influence the particle morphology, but the particles appeared to be smoother, and coalescence of the rhodium particles was observed at 400 °C. The Rh dispersions calculated for

the samples pretreated at 400 °C were 15.5% for FM, 20.1% for DG and 9.3% for EH. Note that these values represent apparent dispersions, because it is not clear whether all of the rhodium was reduced even at 400 °C (vide infra).

Fig. 5 depicts the reduction progress as a function of temperature for the three catalytic materials. Reduction was virtually complete at ca. 500 °C for the commercial catalysts, whereas for the flame-made sample, complete reduction was not achieved at this temperature. The difference in the reduction progress between DG and EH indicates that the latter contained significantly more metallic Rh before reduction. On the other hand, the nearly parallel curves in Fig. 5 for DG and EH at temperatures above ca. 280 °C show that the reducibility of the rhodium component was comparable in the two reference materials but strikingly different for FM. Note that the maximal concentration of hydrogen during reduction by pulses in a TA-MS experiment was ca. 1 vol%, two orders of magnitude lower than that achieved during reduction by neat hydrogen in the chemisorption procedure and during catalyst pretreatment. Therefore, a direct comparison of the temperatures of reduction is not straightforward.

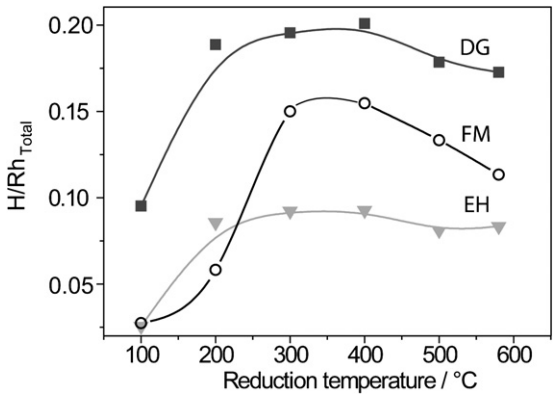

Fig. 4. Hydrogen uptake (referred to total number of Rh atoms) of flame-made and reference Rh/Al_2O_3 catalysts measured after one hour reduction of the samples at specified temperature. Rh dispersions quoted in text were determined from H_2-uptake of catalysts reduced at 400 °C. The lines are drawn to guide the eye.

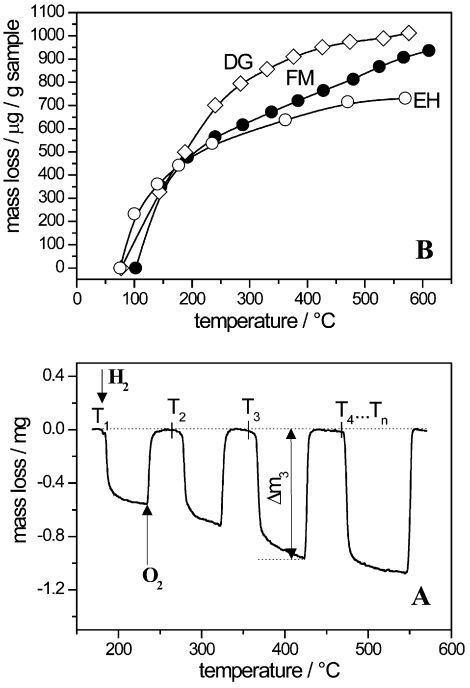

Fig. 5. Reduction/oxidation behavior of flame-made and reference Rh/Al_2O_3 catalysts. (A) Principle of the determination of the dependence Δm vs T: the pulses of H_2 injected at temperatures $T_1 - T_n$ were followed by pulses of oxygen, e.g. the mass loss at the temperature T_3 due to the hydrogen pulse amounts to Δm_3. (B) Mass changes related to 1 g of sample due to 1-ml pulses of hydrogen followed by 2-ml pulses of oxygen at different temperatures.

Adsorption of CO followed by infrared spectroscopy provides information on the state and morphology of the rhodium component, because the adsorption mode of CO is sensitive to different rhodium structures [35]. We investigated FM, DG, and EH at room temperature by DRIFTS both as-received and after reduction at 200 and 400 °C. The infrared spectra of the as-received samples showed a doublet at ca. 2089 and 2016 cm^{-1} (Fig. 6). EH and, to a lesser extent, DG exhibited additional features at 2049 and 1838 cm^{-1}, attributed to on-top and bridge-bonded CO adsorbed on metallic Rh [36], respectively. The pair of signals at ca. 2090 and 2020 cm^{-1} is assigned to *gem* dicarbonyl species and indicate population of cationic rhodium species [35,37,38]. These two signals grew with coverage at constant frequency and thus are attributed to isolated species. The signals evolved rather slowly on the three samples, and evolution of CO_2 also was observed, suggesting morphological changes in the structure of rhodium. The slow evolution of the CO signals with contact time compared with, for example, the reduced samples is associated with the CO-induced disrup-

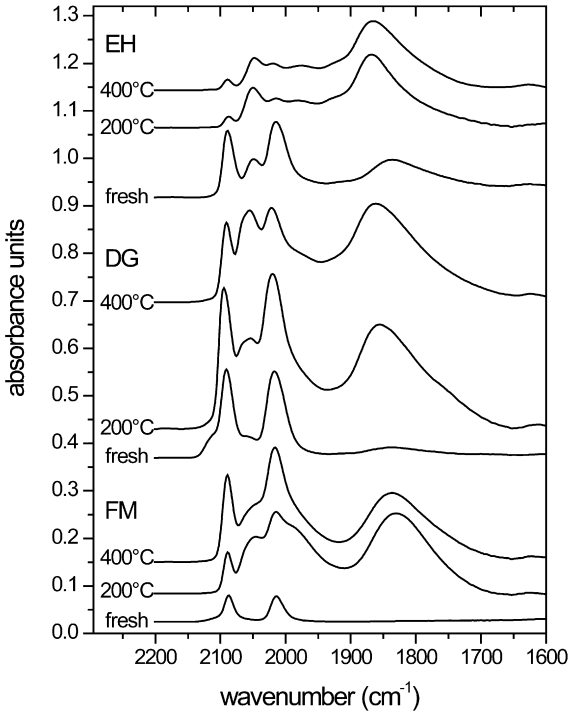

Fig. 6. Room temperature DRIFT spectra of CO adsorption on the Rh/Al_2O_3 samples, as received (fresh) and reduced at 200 and 400 °C, respectively. Spectra are offset for clarity.

tion of Rh–Rh bonds in the metal particles and formation of the cationic species [39]. The order of the amount of evolved CO_2 was EH > DG > FM, which agrees well with the obvious difference observed in the spectra of CO adsorbed on the as-received samples, that is, lower amount of cationic species and practically no Rh crystallites in the FM sample (Fig. 6). The evolution of CO_2 in EH was logically related to the slow growth of the Rh particles, as demonstrated by the continuously increasing signal of bridged CO (not shown in Fig. 6). An additional feature in the spectra of FM and DG at ca. 2110 cm^{-1} suggests the presence of Rh species in a higher oxidation state (+1 and/or +2) that vanishes after H_2 treatment.

The DRIFTS spectrum of FM reduced at 400 °C (Fig. 6) exhibited signals at 2090 and 2020 cm^{-1} and at 2050 and 1840 cm^{-1}, the latter confirming adsorption of CO on metallic Rh particles. Interestingly, reduction of the same sample at 200 °C generated signals of cationic species at the same frequency but with lower intensity. Similar features were observed on flame-made samples with Rh loadings of 0.5–5 wt%, with increased intensity with increasing loading (vide infra). In contrast to FM, and in a more classic fashion, the intensity of these signals decreased with increasing reduction temperature in the case of DG (Fig. 6), in agreement with the higher fraction of Rh in the reduced state at higher reduction temperatures. CO_2 evolution was almost completely suppressed after reduction at 200 °C. All samples reduced at 400 °C also displayed a signal at ca. 1990 cm^{-1}, indicative of bridge-bonded CO on cationic Rh [40]. EH and DG exhibited an additional feature at ca. 1920 cm^{-1}, as reported by Griffiths et al. [41]. The signal at 1990 cm^{-1} exhibited the same behavior as the signals due to the *gem* di-carbonyl species at reduction temperature.

The increased intensity of the signals of cationic Rh species with reduction temperature in the FM sample is likely related to a larger fraction of oxidic rhodium (probably in the form of Rh_2O_3) in the as-prepared material. Fig. 6 suggests that the as-prepared FM sample was composed predominantly of oxidic Rh and that rhodium was in a mixed Rh^0–Rh^+–Rh_2O_3 state in the sample reduced at 400 °C. The prominent signals of the cationic species in FM and DG reveal that dispersion was higher than in EH, in good agreement with the calculated dispersion.

In contrast to FM and DG, EH contained hardly any cationic rhodium after reduction, and the fraction of metallic rhodium was high before reduction, in agreement with the results shown in Fig. 5. In addition, in this sample the on-top-to-bridge intensity ratio was largely in favor of the bridge species, suggesting that Rh particles were larger here than on FM and DG, in agreement with the STEM, XRD, and dispersion data.

The continuously increasing reduction progress with increasing temperature observed for FM and the apparent reverse order of stability of cationic species with respect to DG indicates the presence of rhodium in an oxidized state that is not as easily reducible as in the commercial catalysts. A similar stability against reduction (stable Pd dispersion up to 600 °C) was observed for a flame-made 5 wt% Pd/Al_2O_3, for which no CO adsorption measurements are available, however [6].

The combination of the different characterization methods allows us to attempt to interpret the state of the Rh constituent in FM. The H_2 chemisorption experiments demonstrated marked differences in the reducibility of the Rh-containing surface species in the three catalysts. FM required higher temperatures to obtain an appreciable amount of metallic rhodium, indicating that the rhodium oxide layer was more stable against reduction. A similar stability was found in the reduction experiments by TG (Fig. 5). Both commercial catalysts showed a rapid increase in metallic Rh content at ca. 150 °C (EH) and 200 °C (DG), followed by a slower increase that leveled off within the temperature range investigated. The continuous increase observed in the FM sample might be attributed to the reduction of bulk rhodium oxide, progressing at a lower rate than the reduction of surface rhodium oxide due to diffusion limitations. Together, the data indicate that the Rh in FM was completely oxidized and that this oxidic rhodium was more stable than the rhodium oxide layer in the commercial catalysts.

The high temperature and highly oxidizing environment during flame synthesis and the initially atomically dispersed precursor materials allow the formation of Rh entities in close contact with the Al_2O_3 lattice, although in flame synthesis, generally the refractory component is believed to form before the noble metal particles [8,42]. This intimate contact would allow the Rh or Rh_2O_3 to be stabilized within the alumina matrix [43]. As a result, complete reduction of rhodium oxide in FM requires higher temperatures than those applied in this study (>600 °C). This feature appears to be typical for supported Rh catalysts treated at elevated temperature in oxygen atmosphere [44,45], which agrees well with the high-temperature oxidizing conditions achieved in the FSP process. The degree of intimate metal–support interaction has been found to increase with calcination temperature [43,46], and the growth of Rh particles has been found to be inhibited at high temperatures [47].

Another important feature of FM is the presence of a large fraction of cationic rhodium species, as detected by CO adsorption. The positive charge of the Rh could arise from intimate contact with an oxygen atom from either Al_2O_3 or Rh_2O_3. Partial reduction of the rhodium oxide phase likely results in Rh atoms in close contact with Rh_2O_3, thus allowing for formation of Rh^+ species. Reduction by hydrogen causes a gradual erosion of the rhodium oxide and the appearance of increasing fraction of metallic Rh with increasing reduction temperature. As a result, the amount of Rh^+ species increases within the range of reduction temperature. Note, however, that the maximum achievable amount of accessible metallic rhodium was reached at 400 °C (Fig. 4). The Rh^+ signals at this temperature might originate from both the aforementioned Rh–Rh_2O_3 interaction and an Rh–Al_2O_3 intimate interaction. With particles as small as in the case of FM, a large fraction of Rh atoms will be located at an interface (Rh–Rh_2O_3 and Rh–Al_2O_3).

Both the low reducibility and the amount and stability of cationic Rh species seem to be intrinsic structural properties of the flame-made Rh/Al_2O_3, which appears to be nonreproducible without high-temperature oxidation treatments in analogous materials otherwise synthesized. This feature also could apply more generally to other flame-made supported noble-metal catalysts [6–8,29,48].

3.2. Catalytic properties

The significant differences observed in the state of rhodium and in particle size indicate possible differences in the catalytic behavior of the three catalysts. We tested their performance in the liquid-phase chemoselective and enantioselective hydrogenation of **1** in the absence (racemic hydrogenation) and presence of the chiral modifier cinchonidine (CD). We also investigated the effect of pretreatment temperature on both types of reactions, to gain insight into the possible influence of the content of cationic Rh species on catalytic performance. Fig. 7 shows representative data of the 5 wt% Rh/Al_2O_3 flame-made catalyst and the reference catalysts. As shown, FM was virtually inactive without reductive pretreatment. Reduction at 400 °C before racemic hydrogenation afforded a conversion exceeding that observed with DG and EH by 20–30%. The commercial catalysts did not necessarily need pre-treatment; both catalysts either were already reduced or could be reduced under reaction conditions [20]. These results agree well with the reduction behavior of the three samples. Interestingly, chiral modification by CD greatly enhanced chemoselectivity to >80% but decreased the conversion. The highest conversion again was observed with FM. The *ee* was generally low and did not change significantly after pretreatment for all catalysts. The highest *ee* was obtained with EH, which had a significantly lower dispersion than DG and FM. This behavior is similar to that of platinum-based catalysts, which also display higher *ee* at low dispersion [33, 49–51].

FM with weight loadings of 0.5–5 wt% showed increased conversion, but decreased chemoselectivity and *ee*, with increasing Rh loading (Fig. 8). CO adsorption on these samples indicated that the content of cationic and metallic Rh species also increased with Rh loadings. This is best seen in the behavior of the intensity of the signals at 2090 and 1840 cm^{-1}, which can be taken as a qualitative measure of the fractions of Rh^+ and Rh^0, respectively (top panel of Fig. 8). The ratio of these two signals correlates well with the trend observed in the chemoselectivity of the racemic hydrogenation reaction. The negative slope indicates that the fraction of cationic Rh diminished with increasing Rh loading, reducing their potential influence on the reaction.

Fig. 7 clearly shows that the hydrogen pretreatment greatly affected the performance of FM and was required for the selected chemoselective and enantioselective hydrogenation reaction. To investigate this aspect more deeply, we tested samples pretreated at 100–580 °C in the presence and in the absence of the modifier. The results, shown in Fig. 9, demonstrate that the activity of FM exhibited a significant dependence on the reduction temperature. Conversion exhibited a maximum for the sam-

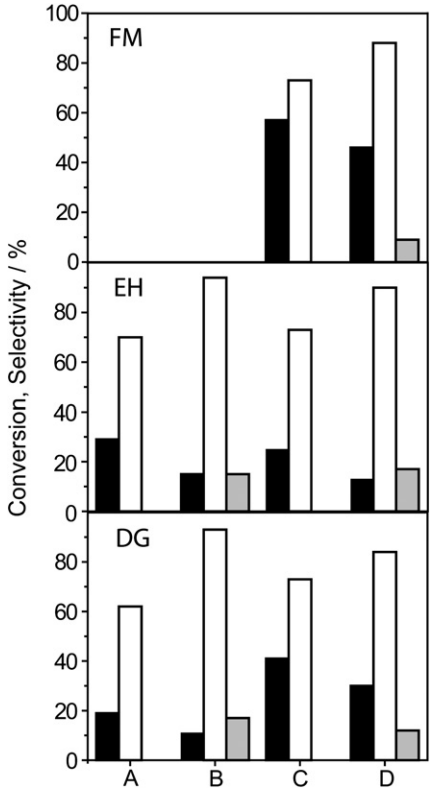

Fig. 7. Overview on the catalytic results in the hydrogenation of (**1**). Black, conversion; white, selectivity to (**2**); gray, *ee*. Reaction conditions: 10 bar hydrogen, 5 mL solvent, 2 mg CD, 42 mg catalyst, 0.33 mL (**1**). (A) No modifier, no pre-treatment; (B) modifier, no pre-treatment; (C) no modifier, pre-treated at 400 °C; (D) modifier, pre-treated at 400 °C.

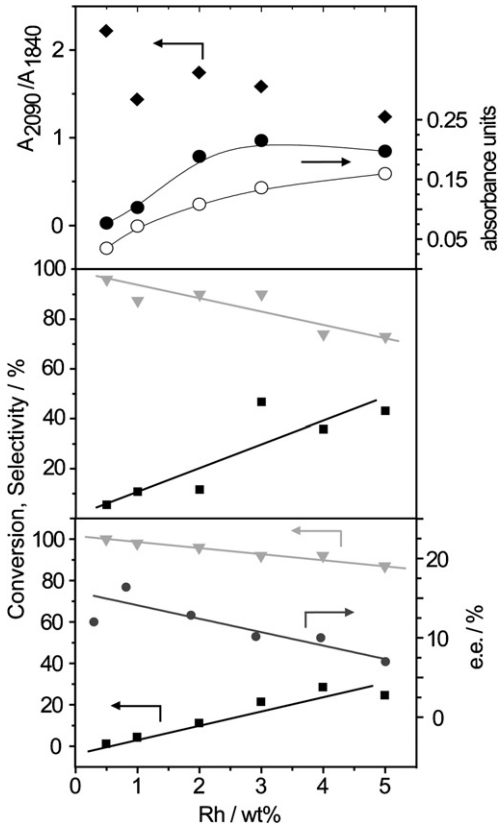

Fig. 8. Top panel: intensities of the signals of adsorbed CO at 2090 and 1840 cm^{-1} representative of cationic (●) and metallic (○) Rh, respectively, and the ratio of these intensities (◆). Lower panels: catalytic behavior of flame-made catalysts in the hydrogenation of (**1**) as a function of rhodium weight loading expressed in terms of conversion (■), chemoselectivity (▼) (left axis) and *ee* (●) (right axis). Reduced at 400 °C, standard reaction conditions. The lines are drawn to guide the eye.

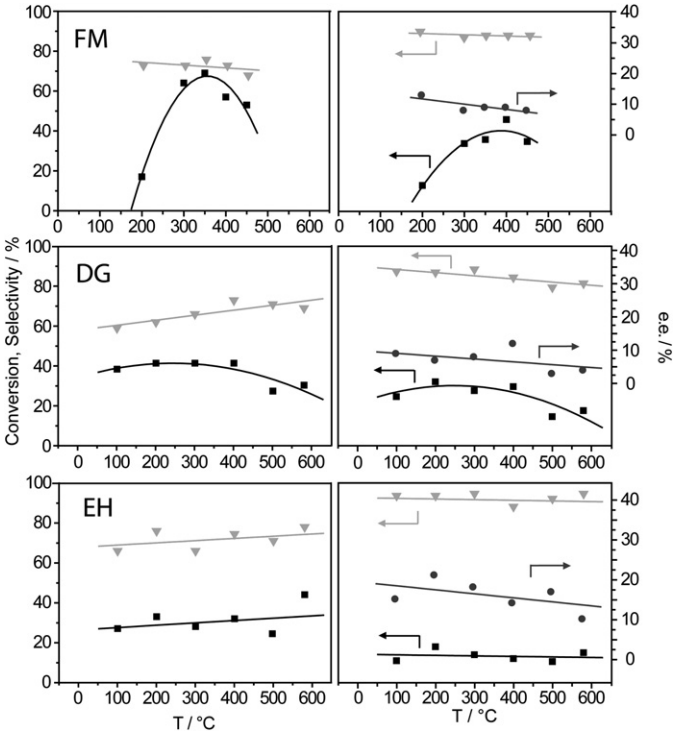

Fig. 9. Influence of pretreatment temperature of Rh/Al_2O_3 catalysts on hydrogenation of (**1**) in terms of conversion (■), chemoselectivity (▼, both left axis) and *ee* (●, right axis). Standard reaction conditions. The lines are drawn to guide the eye.

ples reduced at 350 °C with modifier and 400 °C without modifier. This trend is in agreement with the hydrogen chemisorption experiments (Fig. 4), in which hydrogen uptake increased up to 300–400 °C and then decreased at higher reduction temperatures. Slightly increased conversion with increasing reduction temperature was observed for the unmodified EH catalyst. The trend observed for DG was in between those of FM and EH, supporting the behavior demonstrated in Fig. 5.

Chemoselectivity was higher for the CD-modified catalysts in all cases, regardless of reduction temperature. An almost constant selectivity to **2** was achieved with the unmodified (70%) and modified (90%) FM. DG and EH displayed comparable increases in chemoselectivity with increasing reduction temperature, from about 60% to 70%; however, CD-modified DG showed a slight decrease in chemoselectivity with increasing reduction temperature. The trends in enantioselectivity were similar in all three catalysts, with *ee* dropping from 17% to 9% for FM, from 10% to 4% for DG, and from 15% to 10% for EH.

The strong dependence of conversion on reduction temperature observed in Fig. 9 for FM and, to a lesser extent, for DG correlates well with the fraction of cationic species present on these two samples as detected by CO chemisorption. As mentioned above, oxidic Rh species in FM appeared to be more stable, and reduction still afforded a large fraction of cationic species, resulting in increased concentration of these species with increasing reduction temperature up to 400 °C. The activity of FM exceeded that of the commercial catalysts after reduction at 300 °C (Fig. 9), accompanied by comparable or even superior selectivity. In addition, the trends observed in Fig. 9 correlate well with those shown in Fig. 4 for FM and DG. Although hydrogen uptake was generally higher for DG, the catalytic activity of FM was higher after reduction at 300 °C. These findings suggest that metallic surface area alone may not be decisive in determining catalytic performance, and that cationic Rh species may affect both conversion and chemoselectivity. Strikingly, the decreased fraction of Rh^+ species with increasing Rh-loading (Fig. 8) was accompanied by a corresponding decrease in chemoselectivity. However, the relative amount of cationic species still remained larger in the FM sample than in the reference catalysts. Thus FM, with a large fraction of cationic Rh species, is favored over EH and DG probably because of this particular structural property.

The involvement of cationic species in chemoselective hydrogenations over supported noble metal catalysts is known [17]. Positively charged metal atoms can promote the attack of hydrogen to carbonyl groups, thus promoting C=O bond hydrogenation over C=C bond hydrogenation. Beneficial effects of the presence of cationic species on chemoselectivity have been reported for, for example, Rh/TiO_2 [52], $Rh–Sn/SiO_2$ [53], and $Rh–Ge/Al_2O_3$ [54,55], that is, on samples in which the electronic state of Rh is altered either by a strongly interacting support (TiO_2) or by the addition of a second metal (Sn or Ge). A possible role of cationic Rh species in gas-phase reactions has also been reported [56,57]. In FM, it seems feasible that cationic Rh species influence the hydrogenation properties of the Rh particles.

4. Conclusion

In this study, Rh/Al_2O_3 was prepared by FSP and tested in the liquid-phase chemoselective and enantioselective hydrogenation of 3,5-di-(trifluoromethyl)-acetophenone. Characterization with various complementary methods revealed major differences in the structure and reduction behavior of the rhodium constituent compared with commercial reference catalysts. This behavior was reflected in the catalytic data, indicating that for the flame-made Rh/Al_2O_3 (FM), the activity depends strongly on the reduction temperature, with a maximum at ca. 350–400 °C. Given a reduction at 400 °C, FM proved superior compared to the commercial catalysts DG and EH in terms of both conversion and chemoselectivity. This behavior is attributed to the stable oxidic rhodium phase found on the flame-made Rh/Al_2O_3, which was not completely reduced even at 400 °C. Reduction at increasing temperature afforded an increasing fraction of cationic rhodium species, which, together with the stability of the oxidic phase, may indicate an intimate contact between the flame-made rhodium component and the Al_2O_3 constituent. Although metallic Rh is needed to allow observation of catalytic activity, the observed trends in evolution of cationic species and in conversion and chemoselectivity with reduction temperature suggest that these species may be involved in chemoselectivity as well. A final assessment concerning the possible role of the cationic Rh species in catalytic hydrogenation will require pertinent in situ spectroscopic studies. The likely strong interaction between Rh-phase and Al_2O_3 in FM appears to be a peculiar structural property provided by

the FSP methodology in a single synthesis step and may be characteristic of other supported noble metals prepared by this route as well.

Acknowledgment

Financial support was provided by the Swiss National Foundation and ETH (grant TH 0-20381).

References

[1] S.E. Pratsinis, Prog. Energy Combust. Sci. 24 (1998) 197.
[2] T. Johannessen, J.R. Jenson, M. Mosleh, J. Johansen, U. Quaade, H. Livbjerg, Chem. Eng. Res. Des. 82 (2004) 1444.
[3] R. Strobel, A. Baiker, S.E. Pratsinis, Adv. Powder Technol. 17 (2006) 457.
[4] L. Mädler, H.K. Kammler, R. Mueller, S.E. Pratsinis, J. Aerosol Sci. 33 (2002) 369.
[5] L. Mädler, W.J. Stark, S.E. Pratsinis, J. Mater. Res. 18 (2003) 115.
[6] R. Strobel, F. Krumeich, W.J. Stark, S.E. Pratsinis, A. Baiker, J. Catal. 222 (2004) 307.
[7] R. Strobel, L. Madler, M. Piacentini, M. Maciejewski, A. Baiker, S.E. Pratsinis, Chem. Mater. 18 (2006) 2532.
[8] R. Strobel, W.J. Stark, L. Mädler, S.E. Pratsinis, A. Baiker, J. Catal. 213 (2003) 296.
[9] G.L. Chiarello, I. Rossetti, P. Lopinto, G. Migliavacca, L. Forni, Catal. Today 117 (2006) 549.
[10] W.J. Stark, A. Baiker, S.E. Pratsinis, Part. Part. Syst. Charact. 19 (2002) 306.
[11] W.J. Stark, M. Maciejewski, L. Madler, S.E. Pratsinis, A. Baiker, J. Catal. 220 (2003) 35.
[12] W.J. Stark, S.E. Pratsinis, A. Baiker, J. Catal. 203 (2001) 516.
[13] S. Hannemann, J.-D. Grunwaldt, F. Krumeich, P. Kappen, A. Baiker, Appl. Surf. Sci. 252 (2006) 7862.
[14] R. Strobel, J.-D. Grunwaldt, A. Camenzind, S.E. Pratsinis, A. Baiker, Catal. Lett. 104 (2005) 9.
[15] L. Mädler, W.J. Stark, S.E. Pratsinis, J. Mater. Res. 17 (2002) 1356.
[16] W.J. Stark, J.-D. Grunwaldt, M. Maciejewski, S.E. Pratsinis, A. Baiker, Chem. Mater. 17 (2005) 3352.
[17] P. Mäki-Arvela, J. Háyek, T. Salmi, D.Y. Murzin, Appl. Catal. A: Gen. 292 (2005) 1.
[18] H.-U. Blaser, B. Pugin, F. Spindler, J. Mol. Catal. A: Chem. 231 (2005) 19.
[19] T. Mallat, A. Baiker, in: R.A. Sheldon, H. van Bekkum (Eds.), Fine Chemicals through Heterogeneous Catalysis, Wiley–VCH, Weinheim, 2001.
[20] R. Hess, F. Krumeich, T. Mallat, A. Baiker, J. Mol. Catal. A: Chem. 212 (2004) 209.
[21] M. Maris, T. Mallat, A. Baiker, J. Mol. Catal. A: Chem. 242 (2005) 151.
[22] O.J. Sonderegger, G.M.-W. Ho, T. Bürgi, A. Baiker, J. Catal. 230 (2005) 499.
[23] E. Toukoniitty, S. Franceschini, A. Vaccari, D.Y. Murzin, Appl. Catal. A: Gen. 300 (2006) 147.
[24] Y. Huang, J. Chen, H. Chen, R. Li, Y. Li, L. Min, X. Li, J. Mol. Catal. A: Chem. 170 (2001) 143.
[25] W. Xiong, H. Ma, Y. Hong, H. Chen, X. Li, Tetrahedron: Asymmetry 16 (2005) 1449.
[26] Y. Huang, Y. Li, J. Hu, P. Cheng, H. Chen, R. Li, X. Li, C.W. Yip, A.S.C. Chan, J. Mol. Catal. A: Chem. 189 (2002) 219.
[27] J.-D. Grunwaldt, A. Baiker, Catal. Lett. 99 (2005) 5.
[28] J.-D. Grunwaldt, S. Hannemann, C.G. Schroer, A. Baiker, J. Phys. Chem. B 110 (2006) 8674.
[29] S. Hannemann, J.-D. Grunwaldt, P. Lienemann, D. Günther, F. Krumeich, S.E. Pratsinis, A. Baiker, Appl. Catal. A: Gen. 316 (2007) 226.
[30] K. Foger, in: J.R. Anderson, M. Boudart (Eds.), Catalysis: Science and Technology, vol. 6, Springer, Berlin, 1984, Chapt. 4, p. 257.
[31] S.J. Pennycook, Ultramicroscopy 30 (1989) 58.
[32] M. Maciejewski, C.A. Müller, R. Tschan, W.D. Emmerich, A. Baiker, Thermochim. Acta 295 (1997) 167.
[33] T. Mallat, S. Frauchiger, P.J. Kooyman, M. Schürch, A. Baiker, Catal. Lett. 63 (1999) 121.
[34] G. Rupprechter, G. Seeber, H. Goller, K. Hayek, J. Catal. 186 (1999) 201.
[35] R.R. Cavanagh, J.T. Yates, J. Chem. Phys. 74 (1981) 4150.
[36] A.C. Yang, C.W. Garland, J. Phys. Chem. 61 (1957) 1504.
[37] M. Primet, J. Chem. Soc.-Faraday I (1978) 2570.
[38] F. Solymosi, M. Pasztor, J. Phys. Chem. 89 (1985) 4789.
[39] H.F.J. van't Blik, J.B.A.D. van Zon, T. Huizinga, J.C. Vis, D.C. Koningsberger, R. Prins, J. Phys. Chem. 87 (1983) 2264.
[40] C.A. Rice, S.D. Worley, C.W. Curtis, J.A. Guin, A.R. Tarrer, J. Chem. Phys. 74 (1981) 6487.
[41] I.M. Hamadeh, P.R. Griffiths, Appl. Spectrosc. 41 (1987) 682.
[42] T. Johannessen, S. Koutsopoulos, J. Catal. 205 (2002) 404.
[43] R. Burch, P.K. Loader, N.A. Cruise, Appl. Catal. A: Gen. 147 (1996) 375.
[44] K. Dohmae, T. Nonaka, Y. Seno, Surf. Interface Anal. 37 (2005) 115.
[45] C. Wong, R.W. McCabe, J. Catal. 119 (1989) 47.
[46] C.P. Hwang, C.T. Yeh, Q.M. Zhu, Catal. Today 51 (1999) 93.
[47] D.D. Beck, T.W. Capehart, C. Wong, D.N. Belton, J. Catal. 144 (1993) 311.
[48] R. Strobel, S.E. Pratsinis, A. Baiker, J. Mater. Chem. 15 (2005) 605.
[49] G.A. Attard, K.G. Griffin, D.J. Jenkins, P. Johnston, P.B. Wells, Catal. Today 114 (2006) 346.
[50] J.T. Wehrli, A. Baiker, D.M. Monti, H.-U. Blaser, J. Mol. Catal. 49 (1989) 195.
[51] J.T. Wehrli, A. Baiker, D.M. Monti, H.-U. Blaser, J. Mol. Catal. 61 (1990) 207.
[52] P. Reyes, M.D. Aguirre, I. Melian-Cabrera, M.L. Granados, J.L.G. Fierro, J. Chilean Chem. Soc. 51 (2002) 547.
[53] L. Sordelli, R. Psaro, G. Vlaic, A. Cepparo, S. Recchia, C. Dossi, A. Fusi, R. Zanoni, J. Catal. 182 (1999) 186.
[54] G. Lafaye, T. Ekou, C. Micheaud-Especel, C. Montassier, P. Marecot, Appl. Catal. A: Gen. 257 (2004) 107.
[55] G. Lafaye, C. Mihut, C. Especel, P. Marécot, M.D. Amiridis, Langmuir 20 (2004) 10612.
[56] F. Fajardie, J.F. Tempere, J.M. Manoli, O. Touret, G. Blanchard, G. Djega-Mariadassou, J. Catal. 179 (1998) 469.
[57] M.A. Newton, A.J. Dent, S. Diaz-Moreno, S.G. Fiddy, B. Jyoti, J. Evans, Chem.-Eur. J. 12 (2006) 1975.